New Synthetic Route, Characterization, and Electrocatalytic Activity of Nanosized Manganite

Vincent Mark B. Crisostomo,[||] J. Katana Ngala,[||] Shaun Alia,[‡] Arthur Dobley,[§] Christine Morein,[§] Chun-Hu Chen,[||] Xiongfei Shen,[†] and Steven L. Suib*[,||,‡,†]

Department of Chemistry, University of Connecticut, 55 North Eagleville Road, Unit 3060, Storrs, Connecticut 06269, Department of Chemical, Materials and Biomolecular Engineering, University of Connecticut, 191 Auditorium Road, Unit 3222, Storrs, Connecticut 06269, Yardney Technical Products, Inc., 82 Mechanic Street, Pawcatuck, Connecticut 06379, and Institute of Materials Science, University of Connecticut, 97 North Eagleville Road, Unit 3136, Storrs, Connecticut 06269

Received December 4, 2006. Revised Manuscript Received February 6, 2007

Nanosized γ-MnOOH (manganite) has been synthesized by a new route via the reduction of $KMnO_4$ with sucrose and $MnSO_4$ in acidic medium under refluxing conditions for 4 and 6 h. Characterization of these manganite materials using XRD, FESEM, TEM, TGA, and IR were carried out. The obtained manganite samples using the new route were compared against a conventionally prepared one where synthesis involved the oxidation of $MnSO_4$ with a H_2O_2 solution in a basic medium. Two new synthetic methods were developed, one involving addition of $KMnO_4$ into a solution of both sucrose and $MnSO_4$ while the other involved addition of $KMnO_4$ solution into sucrose only followed by addition of $MnSO_4$ (s). The latter method yielded smaller particles (up to 30 nm) than the former method (up to 80 nm) and the conventionally prepared manganite (up to 50 nm). The synthesized manganite materials exhibited promising characteristics when tested as electrocatalysts in the reduction of O_2. The larger particles gave higher peak currents in CV. When incorporated in Yardney's medium-sized lithium-air battery, the larger particles gave higher specific capacity (up to 2.2 A·h/g), which corresponds to about a 38% increase in specific energy of the battery when compared to a battery where no manganite was incorporated.

1. Introduction

The structural flexibility and unique chemical and physical properties of manganese oxides and oxyhydroxides render them valuable in many technological applications. These manganese-based materials are used as chemical catalysts,[1] molecular sieves,[2] and cathode materials in primary and rechargeable batteries.[3] Bach et al.[4] have pointed out that the electrochemical properties of manganese oxides strongly depend on properties such as morphology, crystalline structure, or bulk density. In the development of low-dimensional structures of manganese oxides, size and dimensionality have been a significant factor in determining the unique properties of these materials.[5,6]

Figure 1 shows the crystal structure of γ-MnOOH (manganite). Manganite is composed of $Mn^{3+}O_6$ octahedra that are edge- and corner-shared, which form a 1×1 tunnel where hydrogen atoms reside. Other forms of MnOOH are α-MnOOH (groutite) and β-MnOOH (feitknechtite). Both of these are also composed of $Mn^{3+}O_6$ octahedra that are edge- and corner-shared but groutite forms a 2×1 tunnel while feitknechtite forms an octahedral layered structure. Ramstedt and Sjoberg[7] noted that γ-MnOOH is the most stable trivalent manganese hydroxide. Previous reports have shown that in mixed valent manganese materials (e.g., birnessite) Mn(III) forms the most reactive redox sites.[8,9] This suggests that γ-MnOOH should be a very important material for applications involving redox chemistry.

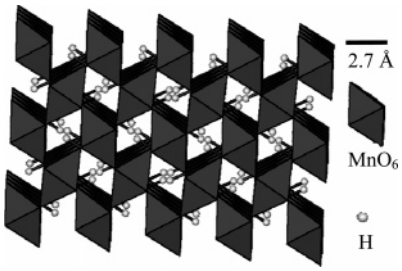

Figure 1. Representation of the crystal structure of γ-MnOOH.

Manganite has been used as a manganese source to produce lithium manganese oxide for lithium ion batteries. A melt impregnation method was employed to prepare

* To whom correspondence should be addressed. E-mail: steven.suib@uconn.edu.
[||] Department of Chemistry, University of Connecticut.
[‡] Department of Chemical, Materials and Biomolecular Engineering, University of Connecticut.
[§] Yardney Technical Products, Inc.
[†] Institute of Materials Science, University of Connecticut.

(1) Yang, Z.; Zhang, Y.; Zhang, W.; Wang, X.; Qian, Y.; Wen, X.; Yang, S. *J. Solid State Chem.* **2006**, *179*, 679.
(2) Hursey, F. X.; Wu, A.; Suib, S. L.; Bushmich, S. L.; Liu, J.; Hincapie, B. PCT Int. Appl. WO 2002*030479*, 2002.
(3) Winter, M.; Brodd, R. J. *Chem. Rev.* **2004**, *104*, 4245.
(4) Bach, S.; Henry, M.; Baffier, N.; Livage, J. *J. Solid State Chem.* **1990**, *88*, 325.
(5) Villegas, J. C.; Garces, L. J.; Gomez, S.; Durand, J. P.; Suib, S. L. *Chem. Mater.* **2005**, *17*, 1910.
(6) Garces, L. J.; Hincapie, B.; Makwana, V. D.; Laubernds, K.; Sacco, A.; Suib, S. L. *Microporous Mesoporous Mater.* **2003**, *63*, 11.
(7) Ramstedt, M.; Sjoberg, S. *Aquat. Geochem.* **2005**, *11*, 413.
(8) Manceau, A.; Drits, V. A.; Silvester, E.; Bartoli, C.; Lanson, B. *Am. Mineral.* **1997**, *82*, 1150.
(9) Nico, P. S.; Zasoski, R. J. *Environ. Sci. Technol.* **2001**, *35*, 3338.

10.1021/cm062871z CCC: $37.00
Published on Web 03/13/2007

$LiMn_2O_{4+y}$ using γ-MnOOH and $LiNO_3$.[10] A hydrothermal treatment of γ-MnOOH in a LiOH solution was reported to produce Li−Mn spinels that showed promising electrochemical behavior.[11] A reflux method was also developed wherein a solution of γ-MnOOH and LiOH was also used producing $LiMnO_2$.[12]

Metal-air batteries are lightweight and have the highest energy density among portable power sources including lithium or metal hydride batteries.[13] This is because O_2 in air is used as one of the active materials. Due to their light weight, metal-air batteries, especially zinc-air batteries, are widely used as a high-capacity power source for hearing aids. The air cathodes are composed of a mixture of carbon powder, O_2 reduction catalysts, and a binder. The performance of these cathodes greatly depends on the constituent materials.

Among the manganese oxyhydroxides, γ-MnOOH, together with other manganese oxides, has been studied as an electrocatalyst in the reduction of O_2 in metal-air batteries.[13−15] These studies report that γ-MnOOH has the highest electrocatalytic activity in O_2 reduction when compared to other manganese oxides (e.g., Mn_2O_3, Mn_3O_4, and Mn_5O_8). In 2003, a mechanistic study by Mao et al.[14] had shown that the electrochemical reduction of O_2 using γ-MnOOH can proceed via a two-electron transfer followed by the γ-MnOOH-catalyzed disproportionation of peroxide produced by the first step electron transfer as shown in eqs 1 and 2.

$$H_2O\,(l) + O_2\,(g) + 2e^- \rightarrow HO_2^-\,(aq) + OH^-\,(aq) \quad (1)$$

$$2HO_2^-\,(aq) \rightarrow 2OH^-\,(aq) + O_2\,(g) \quad (2)$$

γ-MnOOH has been used in combination with cobalt hexadecafluoro-phthalocyanine ($CoPcF_{16}$) to produce a novel alkaline-air electrode with a performance comparable to that of a Pt-based air electrode.[16] The idea of combining $CoPcF_{16}$ with γ-MnOOH to catalytically reduce oxygen was based on Mao et al.'s reported mechanism mentioned above. Ohsaka et al.[15] also described the excellent bifunctional activity of γ-MnOOH in disproportionating superoxide and peroxide anions which are produced when a quinone-like containing electrode reduces oxygen. The above-mentioned mechanism clearly describes the role of γ-MnOOH in O_2 reduction. In view of these significant and recent applications of γ-MnOOH, continuous studies for new routes to prepare γ-MnOOH are important.

Chemical synthesis provides an important approach in terms of controlling properties of manganese oxides. One of these properties is morphology, which can affect catalytic activity of these types of materials. γ-MnOOH has been synthesized through various routes. The most commonly employed synthesis is the oxidation of Mn^{2+} with aqueous H_2O_2 in a basic medium.[17] Nanosized manganite materials have been synthesized by hydrothermal treatment of $KMnO_4$ solutions with various reducing agents such as $(NH_4)_2SO_4$,[18] KI,[19] toluene,[20] and ethanol.[1] Microrods of γ-MnOOH have also been synthesized by a hydrothermal route.[21] Hydrothermal treatment of certain manganese oxide species such as α-MnO_2[22] and β- and γ-MnO_2[23] will produce γ-MnOOH. Other reported synthetic routes also involve hydrothermal treatment of $MnSO_4$ with ethylamine[24] and $NaClO_3$,[25] which yield nanowhiskers and nanostructures of multipods, respectively. A cluster growth route using manganese carboxylate clusters in a basic medium has also been used to produce nanorods of γ-MnOOH.[26] Many of these processes require 12−24 h of reaction time.

In this study, we report a new route to nanosized γ-MnOOH using a reflux process with short times (4 and 6 h) using $KMnO_4$, $MnSO_4$, and sucrose in an acidic medium. The above-mentioned principle, stated by Bach et al. concerning the dependence of electrochemical properties of manganese oxides upon morphology, crystalline structure, and bulk density, can be applied to the new manganite materials produced in our study. We investigated the use of the synthetic materials as electrocatalysts in Yardney's medium-sized lithium-air battery.

2. Experimental Section

2.1. New Synthetic Route to γ-MnOOH. Two similar routes were developed. In **Route 1**, a solution of 5.89 g of $KMnO_4$ in 200 mL of deionized (DI) water was slowly added to a stirred solution of 2.0 g of sucrose, 4.40 g of $MnSO_4{\cdot}H_2O$, 30 mL of water, and 3.0 mL of concentrated HNO_3. The resultant solution was refluxed at 100 °C under constant stirring for 4 (sample **4**) and 6 (sample **6**) hours. In **Route 2**, $MnSO_4{\cdot}H_2O$ was added *last* (or after all the $KMnO_4$ had been added). The resultant solution was also refluxed at 100 °C for 4 (sample **4last**) and 6 (sample **6last**) hours. After hot filtration, the brown solid product was heavily washed with DI water and air-dried.

Variation of Reaction Conditions. Reaction parameters (composition of starting materials, reaction time, and temperature) were exclusively varied to study their effect on the obtained γ-MnOOH. The amount of sucrose (sample **2xSuc**), $KMnO_4$ (sample **2xMn7**+), and $MnSO_4$ (sample **2xMn2**+) were doubled in separate reaction

(10) Xia, Y.; Yoshio, M. *J. Power Sources* **1995**, *57*, 125.
(11) Kanasaku, T.; Amezawa, K.; Yamamoto, N. *Solid State Ionics* **2000**, *133*, 51.
(12) Chitrakar, R.; Kanoh, H.; Miyai, Y.; Ooi, K. *Ind. Eng. Chem. Res.* **2001**, *40*, 2054.
(13) Mao, L.; Sotomura, T.; Nakatsu, K.; Koshiba, N.; Zhang, D.; Ohsaka, T. *J. Electrochem. Soc.* **2002**, *149*, A504.
(14) Mao, L.; Zhang, D.; Sotomura, T.; Nakatsu, K.; Koshiba, N.; Ohsaka, T. *Electrochim. Acta* **2003**, *48*, 1015.
(15) Ohsaka, T.; Mao, L.; Arihara, K.; Sotomura, T. *Electrochem. Commun.* **2004**, *6*, 273.
(16) Mao, L.; Arihara, K.; Sotomura, T.; Ohsaka, T. *Electrochim. Acta* **2004**, *49*, 2515.
(17) Ramstedt, M.; Andersson, B. M.; Shchukarev, A.; Sjöberg, S. *Langmuir* **2004**, *20*, 8224.
(18) Zhang, Y.; Liu, Y.; Guo, F. *Rengong Jingti Xuebao* **2006**, *35*, 705.
(19) Xi, G.; Peng, Y.; Zhu, Y.; Xu, L.; Zhang, W.; Yu, W.; Qian, Y. *Mater. Res. Bull.* **2004**, *39*, 1641.
(20) Zhang, Y. C.; Qiao, T.; Hu, X. Y.; Zhou, W. D. *J. Cryst. Growth* **2005**, *280*, 652.
(21) Zhang, Y.; Liu, Y.; Guo, F.; Hu, Y.; Liu, X.; Qian, Y. *Solid State Commun.* **2005**, *134*, 523.
(22) Yang, R.; Wang, Z.; Dai, L.; Chen, L. *Mater. Chem. Phys.* **2005**, *93*, 149.
(23) Yuan, Z. Y.; Ren, T. Z.; Du, G. H.; Su, B. L. *Appl. Phys. A* **2005**, *80*, 743.
(24) Sun, X.; Chunlai, M.; Wang, Y.; Li, H. *Inorg. Chem. Commun.* **2002**, *5*, 747.
(25) Zheng, D.; Yin, Z.; Weimim, Z.; Tan, X.; Sun, S. *Cryst. Growth Des.* **2006**, *6*, 1733.
(26) Folch, B.; Larionova, J.; Guari, Y.; Guerin, C.; Reibel, C. *J. Solid State Chem.* **2005**, *178*, 2368.

batches using **Route 1** for 24 h at 100 °C. Twelve-hour (sample **12last**) and 24-h (sample **24last)** reaction times were also carried out using **Route 2** at 100 °C to see the effect of reaction time on the morphology and structure of produced manganite. Synthesis using **Route 1** for 24 h was carried out at room temperature or 27 °C (sample **24-RT**), 60 °C (sample **24-60C**), and 100 °C (sample **24-100C**) to study the effect of temperature in the reaction.

Synthesis of Conventional γ-MnOOH. For comparison, γ-MnOOH was also conventionally prepared as reported by Ramstedt et al.[17] (sample **Conv-MnOOH**). In this preparation, 150 mL of 0.2 M NH_3 was added to a solution of 10.2 mL of 30% H_2O_2 and 500 mL of 0.06 M $MnSO_4$. The mixture was refluxed at 100 °C for 6 h under constant stirring. After hot filtration, the brown solid was heavily washed with DI water and air-dried.

2.2. Characterization. *Structure and Morphology.* The structure of the prepared materials was analyzed by X-ray diffraction (XRD) using either a ThermoARL Xtra or a Scintag XDS 2000 X-ray Diffractometer both equipped with a Cu Kα X-ray source (λ = 1.54 Å). The crystal structure and morphology were also analyzed by low- and high-resolution transmission electron microscopy (TEM). Low-resolution TEM was done using a Philips EM420 TEM with an accelerating voltage of 120 kV. High-resolution TEM was done using a JEOL 2010 FasTEM with an accelerating voltage of 200 kV. TEM samples were prepared by suspending the powdered material in 2-propanol, placing a drop of this suspension on a holey carbon-coated copper grid, and evaporating the alcohol. The morphology was also examined by field emission scanning electron microscopy (FESEM) using a Zeiss DSM 982 Gemini FESEM instrument with a Schottky emitter. The sample preparation was the same as that for TEM except that a drop of the suspension was placed on a gold-coated silicon wafer.

Surface Area. A Micromeritics ASAP 2010 instrument was used to measure the Brunauer−Emmett−Teller (BET) surface area of the synthesized materials. Samples were degassed at 120 °C for at least 2 h and the BET surface areas were obtained from nitrogen adsorption data at −196 °C.

Infrared Spectroscopy. The synthesized materials were also characterized by Diffuse Reflectance Fourier Transform Infrared Spectroscopy using a Thermo Nicolet Nexus 670 FTIR instrument equipped with a DTGS detector. Samples were prepared by mixing manganite powders with KBr in an agate mortar. A total of 32 scans per sample was taken with a resolution of 4 cm^{-1}.

Thermal Stability. The thermal stability of the materials was studied by performing thermogravimetric analyses. TGA was carried out on a Hi-Res TGA 2950 thermogravimetric analyzer with a 60 mL/min air flow from room temperature to 1000 °C at a heating rate of 10 °C/min.

2.3. Electrocatalytic Activity. *Cyclic Voltammetry.* Gas-diffusion electrodes were prepared to study the ability of samples **4last**, **4**, **6last**, **6**, **24-60C**, **24-100C**, and **Conv-MnOOH** to reduce oxygen by cyclic voltammetry. Samples were prepared by mixing manganite and carbon powder in a 1:1 ratio. Five drops of 25 wt % PTFE was then added after which the mixture was suspended in water and sonicated. A 1 cm × 1 cm XR 72 carbon paper was coated with the prepared suspension. After the water was evaporated off, the carbon powder, manganite, and binder net weight that was coated was 1 mg for all the samples. The cell setup consisted of the sample mixture on carbon paper as the working electrode, an SCE reference electrode, a Pt counter electrode, and a 1.0 M KOH solution as the electrolyte. A computer-controlled CHI 430 Electrochemical Workstation was used to obtain cyclic voltammograms and a scan rate of 50 mV/s was used. In a typical experiment, the cell was first purged with $N_{2(g)}$ for 30 min followed by an initial scan and then the cell was purged with $O_{2(g)}$ for 30 min and scanned again. Similar CV experiments were carried out where the scan rate was varied (10, 25, and 100 mV/s). The O_2 reduction peak is not limited by the scan rate for the system used in the CV experiments as well as the battery testing (described below) where γ-MnOOH is mixed with carbon powder and binder. So for the purpose of this report, we will only refer to CV under a scan rate of 50 mV/s.

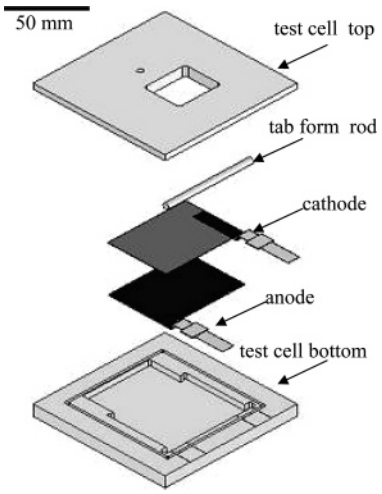

Figure 2. Diagram of a medium-sized lithium-air battery designed by Yardney.

Li-Air Battery Testing. The five manganite samples tested for CV was used as a cathode component to catalyze $O_{2(g)}$ (from air) reduction in a lithium-air battery. Testing was done in triplicate samples obtained from different synthetic batches. For this study, Yardney's medium-sized lithium-air cells were used. Figure 2 shows the diagram of the cell construction. The anode that was used is a pure lithium metal foil with a thickness of 0.08 mm (3 mil). The foil was pressed onto a Ni metal current collector. The current collector was composed of an expanded nickel mesh welded to a nickel tab. Cathodes were made using the hand coating process. The oxygen cathode is a multilayer structure made by combining carbon, manganite, and a binder. This mixture was then impregnated into a nonwoven carbon mat. The carbon mat was then wrapped around a Ni current collector and the multilayer structure was laminated. The final step in the fabrication of the cathode is addition of a microporous PTFE layer to the side exposed to the gaseous environment. The medium cell operates with a cathode of about 13.5 cm^2, which is slightly larger in size than the anode. The separator that was used was a plastic Setela porous membrane. The thickness of the separator was 20 μm. After all the components were prepared, they were layered into a plastic cell case. The cell was then closed and 1.5 mL of electrolyte was added. The liquid electrolyte consisted of a solution of 1 M $LiPF_6$ in 1:1:1 volume EC/DEC/DMC (where EC is ethylene carbonate, DEC is diethyl carbonate, and DMC is dimethyl carbonate). Each cell was placed into a controlled gas environment. The cells were tested under dry $O_{2(g)}$ at 1 atm and at 25 °C. The test profile consisted of an initial 2 h monitored rest, followed by a discharge at a current density of 0.15 mA/cm^2 to a voltage cutoff of 1.5 V and ended with a 2 h final rest.

3. Results and Discussion

3.1. Synthesis. Addition of the solution of $KMnO_4$ to the solution of sucrose and $MnSO_4$ yielded a dark brown slurry. To produce the γ-MnOOH phase, both sucrose and $MnSO_4$ must be present. Absence of sucrose will yield cryptomelane K-OMS2 while the absence of $MnSO_4$ will yield a black

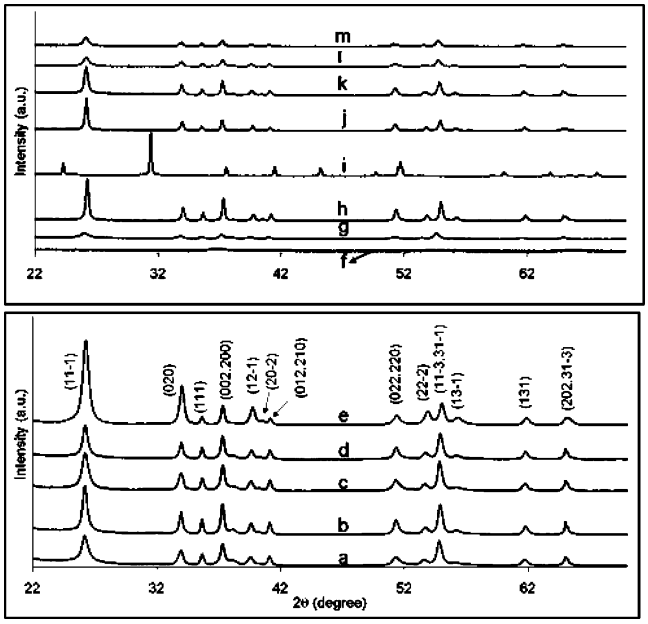

Figure 3. X-ray diffraction patterns of samples (a) **4last**, (b) **4**, (c) **6last**, (d) **6**, (e) **Conv-MnOOH**, (f) **24-RT**, (g) **24-60C**, (h) **24-100C**, (i) **2xSuc**, (j) **2xMn7+**, (k) **2xMn2+**, (l) **12last**, and (m) **24last**.

powder of poor crystallinity. This appears to be the first time that γ-MnOOH was synthesized in a very acidic medium (pH < 1). Manganite has been known to dissolve in acidic media via an acidic disproportionation to Mn^{2+} and MnO_2 according to (3).

$$2\gamma\text{-MnOOH (s)} + 2H^+ \text{(aq)} \leftrightarrows MnO_2 \text{(s)} + Mn^{2+} \text{(aq)} + 2H_2O \text{(l)} \quad (3)$$

This reaction was not observed here. This is because Mn^{2+} is initially present in significantly high concentration. Klewicki and Morgan reported that, at pH below 6.5, the above disproportionation is energetically favorable if $[Mn^{2+}]$ is less than or equal to 10^{-6} M.[27] In our synthesis, the initial $[Mn^{2+}]$ is 0.11 M. Ramstedt and Sjoberg[7] performed experiments on γ-MnOOH acid dissolution and reported that significant dissolution or disproportionation of γ-MnOOH occurs in a time scale of days where formation of ramsdellite occurs in 1 week and then rearrangement to pyrolusite in months whereas our synthesis times involved 4 and 6 h.

3.2. Characterization. All of the reflections in the XRD patterns of the synthesized manganite shown in Figure 3 can be readily indexed to the monoclinic phase of γ-MnOOH (space group $P2_1/c$ (No. 14)) according to JCPDS File No. 41-1379. For the four new manganite samples (**4last**, **4**, **6last**, and **6**, Figures 3a−d), their intensities of reflection for the $(11\bar{1})$ and $(22\bar{2})$ planes are significantly lower than that of **Conv-MnOOH**. This lower intensity might be attributed to the inherent shorter particles (if the particles are considered as having nanorod-like morphologies) of the four new manganite materials when compared to that of **Conv-MnOOH** as evident from FESEM micrographs shown in Figure 4. Yuan et al.[23] also observed variation of the intensity of the $(11\bar{1})$ plane of γ-MnOOH with reaction temperature and time and type of starting materials. The (020) peak intensities for the four samples are lower than that of **Conv-MnOOH**, which might indicate that crystal growth for former materials is different from that of the latter due to the absence of the preferred orientation in this plane which was reported by Dachs.[28]

FESEM micrographs in Figure 4 show the nanometer size of all the synthesized manganite materials. Whereas the **Conv-MnOOH** particles appear as uniformly long fibers (up to 1000 nm), **4last** and **6last** appear as short particles with beanlike shapes (up to 60 and 80 nm, respectively). Samples **4** and **6** are nonuniform particles composed mainly of two types, smaller ones (up to 20 nm) with irregular shapes and bigger (up to 80 nm) ones with rodlike nanomaterials. Morphology and structure of the four materials were further investigated using low- and high-resolution TEM (Figure 5). The samples, though composed of different sizes and shapes, can be considered as the same manganite phase. A selected area electron diffraction pattern is shown for sample **4**. This indicates the single crystallinity of the material, together with no amorphous particles being observed with TEM. Figure 5d shows an HRTEM micrograph of **6** and a simulated electron diffraction pattern. The spacing of the lattice fringes

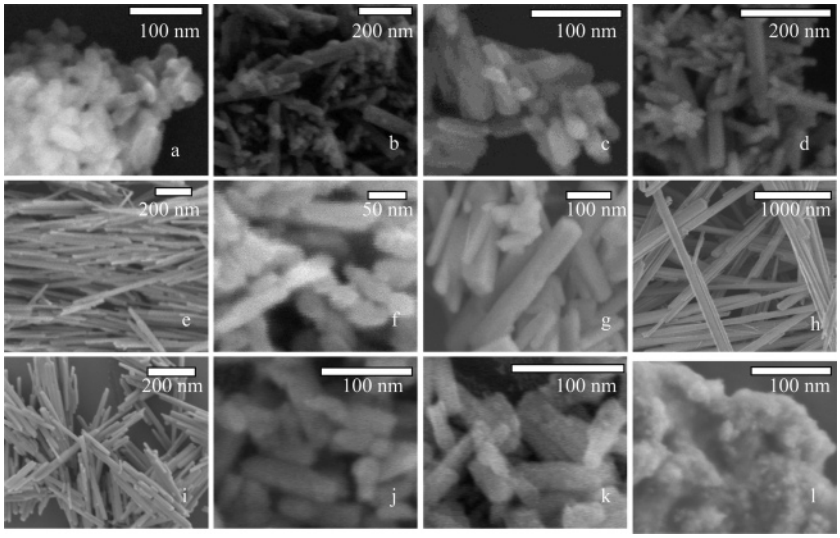

Figure 4. FESEM micrographs of samples (a) **4last**, (b) **4**, (c) **6last**, (d) **6**, (e) **Conv-MnOOH**, (f) **24-60C**, (g) **24-100C**, (h) **2xMn7+**, (i) **2xMn2+**, (j) **12last**, (k) **24last**, and (l) **24-RT**.

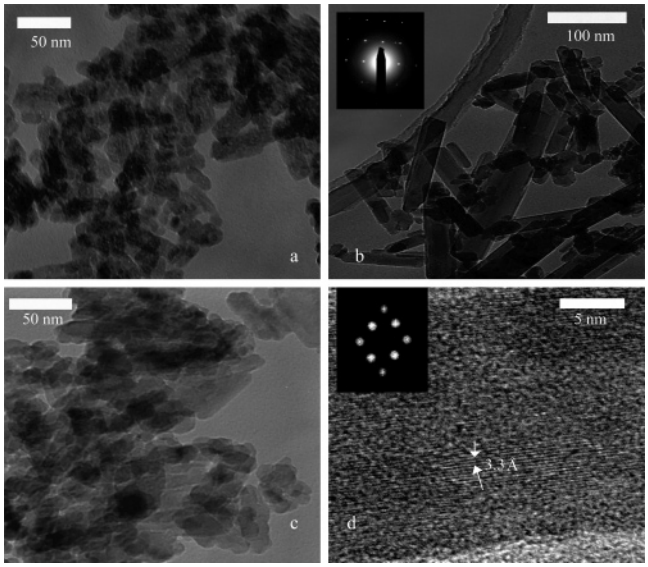

Figure 5. TEM images of samples (a) **4last**, (b) **4** (inset SAED), (c) **6last**, and (d) **6** (inset simulated SAED).

Table 1. Particle Size and BET Surface Area of Synthesized γ-MnOOH

sample	particle length[a] (nm)	particle width[a] (nm)	BET surface area[b] (m^2/g)
Conv-MnOOH	250−1000	15−40	44
4last	25−60	10−30	63
4	70−300	10−80	43
6last	20−80	10−30	62
6	30−250	20−50	41
24-RT	c	c	c
24-60C	20−70	10−20	75
24-100C	70−500	10−60	28
2x-Suc	d	d	d
2x-Mn7+	2000−6000	50−200	17
2x-Mn2+	100−1000	30−60	22
12last	40−200	20−40	44
24last	40−250	20−50	42

[a] Estimated by SEM and TEM micrographs. [b] Standard deviation ± 1. [c] An amorphous manganese oxide was produced. [d] $MnCO_3$ was produced.

(3.3 Å) shown in Figure 5d closely corresponds to the $(11\bar{1})$ plane.

Samples **4**, **6**, and **Conv-MnOOH** have very similar BET surface areas (43, 41, and 44 m^2/g, respectively). Samples **4last** and **6last** have higher surface areas (63 and 63 m^2/g) than the three former ones. These values correspond to the sizes of the materials (estimated from FESEM and TEM micrographs) as shown in Table 1. Whereas the particle sizes of samples **4**, **6**, and **Conv-MnOOH** could go up to 250−1000 nm, the particle sizes for **4last** and **6last** range from 10 to 80 nm. Considering the preparation methods for the four new manganite materials could explain these sizes (and hence surface areas). In samples **4** and **6** (**Route 1**), the $KMnO_4$ solution was slowly added into the solution of sucrose and $MnSO_4$ which favors crystal growth, hence giving larger particles. For **4last** and **6last** (**Route 2**), the $KMnO_4$ solution was slowly added into the sucrose solution and afterward the $MnSO_4$ powder, which facilitates a faster nucleation, was finally added; hence, crystals did not grow much. The two new synthetic routes were repeated to test their reproducibility. Structural and morphological characteristics of the new manganite samples were reproducible.

Variation in reaction temperature and time and composition of starting materials were carried out and the structural and morphological characteristics were studied. γ-MnOOH phase was obtained in all of these variations except for **24-RT** and **2x-Suc** (Figure 3f−m). An amorphous form of manganese oxide (**24-RT**) was obtained when the reaction temperature was lowered to 27 °C (room temperature) as can be seen in Figures 3f and 4l. The crystallinity of manganite obtained when the reaction temperature was 60 °C (**24-60C**) appears to be lower than manganite produced at 100 °C (**24-100C**) as can be seen from the XRD pattern in Figure 3g,h. Crystal growth seems to be favored at higher reaction temperature.

The particle size of sample **24-60C** (up to 70 nm in length) is significantly lower than that of **24-100C** (up to 500 nm in length). This particle size difference is consistent with the BET surface area for **24-60C** (75 m^2/g) and **24-100C** (28 m^2/g). Manganese carbonate was obtained when the amount of sucrose was doubled (**2x-Suc**) as shown in the XRD pattern in Figure 3i ($MnCO_3$, JCPDS File No. 07-0268). Mn^{7+} in the solution was (over)reduced to Mn^{2+} due to the excess reducing sugar. Particle size increased when the amount of $MnSO_4$ and $KMnO_4$ was doubled. Particle lengths of up to 1000 and 6000 nm were obtained for samples **2x-Mn2+** and **2x-Mn7+**, respectively, compared to up to 500 nm for sample **24-100C** where neither of the two reagents were doubled.

A decrease in BET surface area that corresponds to the increase in particle size observed in **2x-Mn2+** (22 m^2/g) and **2x-Mn7+** (17 m^2/g) was observed when compared to that of **24-100C**. This demonstrates the effect of the concentration in particle growth. More concentrated reactants will produce larger crystals, as is the case in many crystallization or precipitation systems. Increasing the reaction time to 12 (**12last**) and 24 (**24last**) hours also resulted in increase in particle length of up to 200 and 250 nm, respectively, compared to 60 and 80 nm for samples **4last** and **6last**, respectively. This increase in particle length upon increase in reaction time correspondingly resulted in a decrease in BET surface area of 44 and 42 m^2/g. This particle size reduction is expected since longer reaction time allows for longer time for crystal growth and therefore larger particles.

The four new manganite samples (**4last**, **4**, **6last**, and **6**) have the same IR spectral features as **Conv-MnOOH** as shown in Figure 6. The broad bands at ca. 1590 and 3500 could be attributed to absorbed water and carbon dioxide because nanocrystalline materials exhibit high surface:volume ratio. The broad band around 2700 cm^{-1} is the fundamental O−H stretching mode belonging to a hydrogen bond with an O−H...O length of ∼2.60 Å in the structure of manganite as reported by Kohler and Armbruster.[29] The three O−H bending modes (γ-OH, δ-2-OH, and δ-1-OH) are observed

(27) Klewicki, J. K.; Morgan, J. J. *Geochim. Cosmochim. Acta* **1999**, *63*, 3017.
(28) Dachs, H. *Z. Krist.* **1963**, *118*, 303.
(29) Kohler, T.; Armbruster, T. *J. Solid State Chem.* **1997**, *133*, 486.

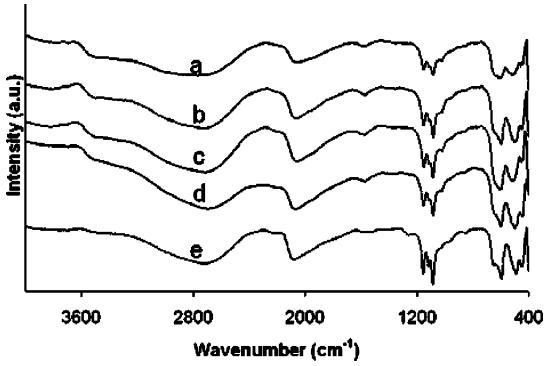

Figure 6. Diffuse reflectance infrared spectra of samples (a) **4last**, (b) **4**, (c) **6last**, (d) **6**, and (e) **Conv-MnOOH** mixed with KBr.

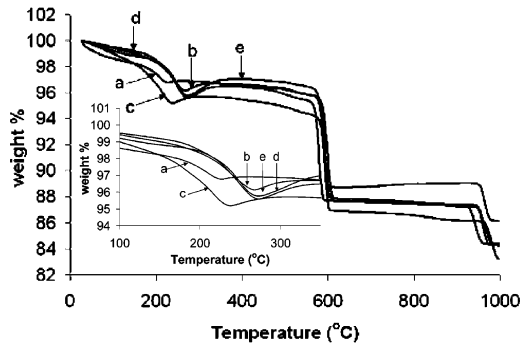

Figure 7. TGA plots obtained in air at a heating rate of 10 °C/min for samples (a) **4last**, (b) **4**, (c) **6last**, (d) **6**, and (e) **Conv-MnOOH**.

at around 1000−1150 cm^{-1}. The peaks below 700 cm^{-1} (650, 600, 500, and 450 cm^{-1}) correspond to lattice Mn−O vibrations. The absorption band at ∼2100 cm^{-1} (*f*) was observed previously in studies of manganite.[20] This band can be considered as a combination band of the OH stretching mode at 2700 cm^{-1} (f_1) and the excited lattice mode at 600 cm^{-1} (f_2), that is, $f = f_1 - f_2 = 2700-600 = 2100$ cm^{-1}. Thus, all the FTIR spectra are in accordance with those of γ-MnOOH reported in the literature.[20,29]

Figure 7 shows the TGA plots obtained for the four manganite samples (**4last**, **4**, **6last**, and **6**). The first weight loss corresponds to the oxidation of γ-MnOOH to β-MnO_2 (pyrolusite) according to (4):

$$4\gamma\text{-MnOOH (s)} + O_2\text{ (g)} \rightarrow 4\beta\text{-}MnO_2\text{ (s)} + 2H_2O\text{ (g)} \quad (4)$$

There is a slight difference in the inflection point (transition temperature) between the manganite samples. Samples **Conv-MnOOH**, **4**, and **6** exhibited transition temperatures at ∼230 °C while **4last** and **6last** show an inflection point at ∼200 °C (inset in Figure 7). This might suggest that the latter two samples are more easily converted to pyrolusite. To confirm the conversion of the synthesized materials according to reaction 2, samples were heated in air at 300 °C for 4 h and XRD patterns were obtained (Figure 8). All the reflections in Figure 8 are consistent with the tetragonal β-MnO_2 phase (JCPDS File No. 24-0735). The morphology of the obtained pyrolusite did not show any marked difference when compared to that of the original γ-MnOOH samples (FESEM micrographs not shown). This preservation of morphology was also reported in other studies.[1,26] Slightly lower weight loss was observed for samples synthesized using **Route 1**

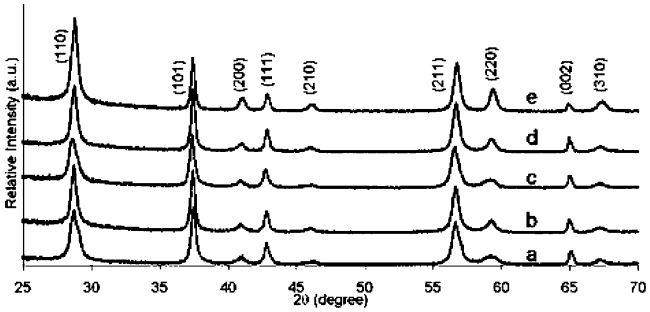

Figure 8. X-ray diffraction patterns of samples (a) **4last**, (b) **4**, (c) **6last**, (d) **6**, and (e) **Conv-MnOOH** after heating at 300 °C in air for 4 h.

(3.7% and 3.8% for **4** and **6**, respectively) when compared to the smaller manganite particle obtained from **Route 2** (4.1% and 5.1% for **4last** and **6last**, respectively). This may be attributed to a greater amount of water absorbed as evident from IR data mentioned above by the former samples due to their larger surface area. The second and third weight loss steps with inflection points ∼590 and ∼950 °C correspond to oxygen release and transformation of β-MnO_2 to Mn_2O_3 according to (5) and the subsequent conversion of Mn_2O_3 to Mn_3O_4 according to (6),[26] respectively:

$$6MnO_2\text{ (s)} \rightarrow 3Mn_2O_3\text{ (s)} + {}^3/_2O_2\text{ (g)} \quad (5)$$

$$3Mn_2O_3\text{ (s)} \rightarrow 2Mn_3O_4\text{ (s)} + {}^1/_2O_2\text{ (g)} \quad (6)$$

3.3. Electrocatalytic Activity. Figure 9 shows the obtained cyclic voltammograms for samples **4**, **4last**, **6**, **6last**, **24-60C**, **24-100C**, and **Conv-MnOOH**. The voltammograms obtained in a N_2 atmosphere show that γ-MnOOH is electrochemically inactive in the potential window and scan rate used in this study. This is shown by data in Figures 9a′, 9b′, 9c′, 9d′, 9e′, 9f′, and 9g′. Upon saturation of the electrolyte with O_2, oxygen reduction potentials and peak currents were obtained as listed in Table 2. The O_2 reduction potentials obtained here closely correspond to those observed in the literature.[30]

Peak currents are a measure of the electrocatalytic activity of γ-MnOOH. Mao et al.[13] demonstrated how electrocatalytic activity of manganese oxides in reducing oxygen can be evaluated by using peak currents. The method that Mao et al. used to determine the peak currents from cyclic voltammograms was employed in our study. Sample **24-100C** (6.4 mA) exhibited the highest current peak followed by samples **6** (6.0 mA) and **4** (5.0 mA). The three samples that had the highest surface area, **24-60C**, **4last**, and **6last**, had lower peak currents (1.9, 2.7, and 4.0 mA, respectively). Whereas increase in surface area would usually result in increased catalytic activity,[31] the results reported here gave the opposite correlation between particle size or surface area and catalytic activity. The electrocatalytic activity seems to be indirectly related to the preparation method. The resulting γ-MnOOH lattice formed may have more active sites when nucleation is slow and crystals are allowed to grow (**Route 1**) when

(30) Kinoshita, K. *Electrochemical Oxygen Technology*; Wiley-Interscience: New York, 1992.
(31) Ngala, J. K.; Alia, S.; Dobley, A.; Crisostomo, V. M. B.; Suib, S. L. *Chem. Mater.* **2007**, *19*, 229−234.

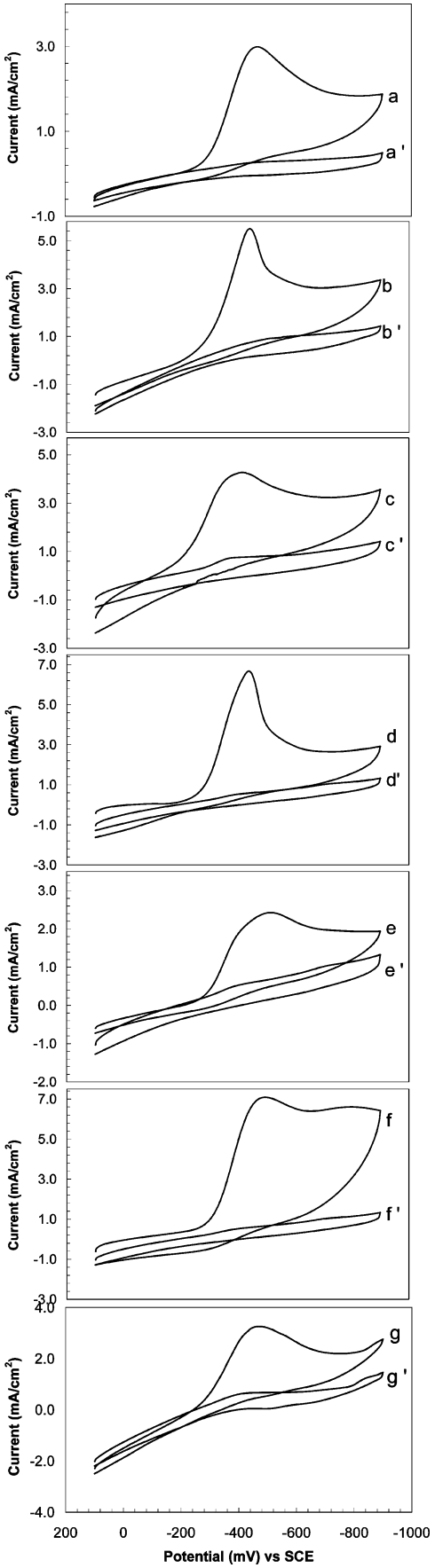

Figure 9. Cyclic voltammograms obtained at a rate of 50 mV/s using samples (a) **4last**, (b) **4**, (c) **6last**, (d) **6**, (e) **24-60C**, (f) **24-100C**, and (g) **Conv-MnOOH** in carbon powder. Curves a′, b′, c′, d′, e′, f′, and g′ were obtained in N_2-purged 1.0 M KOH solution while curves a, b, c, d, e, f, and g were recorded in an O_2-saturated 1.0 M KOH solution.

Table 2. Reduction Potentials,[a] Peak Currents,[a,b] and Specific Capacities of Synthesized γ-MnOOH

sample	reduction potential vs SCE (mV)	current peak (mA)	specific capacity[c] (A·h/g)
24-100C	−479	6.4	d
6	−445	6.0	2.2
4	−446	5.0	1.9
6last	−425	4.0	1.8
Conv-MnOOH	−476	3.0	1.6
4last	−470	2.7	1.3
24-60C	−477	1.9	d

[a] Obtained from O_2-saturated cyclic voltammograms. [b] Measured according to a method described by Mao et al.[13] [c] Average standard deviation ± 0.2. [d] Not done.

compared to that of **Route 2** where crystals did not grow much. The particle shape and size of γ-MnOOH affect the way these particles are dispersed in carbon powder and binder used in sample preparation. Larger particles favor a better dispersion where more of the γ-MnOOH is exposed and readily available for catalysis. Most likely, the new manganite materials (especially samples **4** and **6**) have available surfaces that are unique due to the above-mentioned difference in preferred orientation of these materials when compared to **Conv-MnOOH**. These surfaces may have more active redox sites as compared to that of **Conv-MnOOH**.

γ-MnOOH has been reported to have the highest activity in the electrocatalytic reduction of O_2 of many manganese oxides (e.g., Mn_2O_3, Mn_3O_4, and Mn_5O_8).[13] Mechanistic studies reported by Mao et al.[13] clearly established that γ-MnOOH catalyzes the chemical decomposition according to eq 2. The generated O_2 in (2) is again re-reduced; hence, peak currents for the two-electron O_2 reduction increases. In a separate experiment, peroxide was shown to be decomposed by the synthesized γ-MnOOH. Although γ-MnOOH is known to be a poor conductor, Calegaro et al.[32] alluded to the possibility of a partial dissolution of γ-MnOOH in cyclic voltammetry experiments to produce MnO_2 and Mn^{2+}.

Electrocatalytic activities of samples were also tested in a lithium-air battery. Table 2 lists the specific capacities obtained. The trend in specific capacity follows that of the trend in peak current; that is, higher peak currents (**4** and **6**) give higher specific capacities, confirming the relationship between peak currents and the electrocatalytic activity of the material. An experiment in which carbon alone was used in the cathode and machine coating was employed gave a specific capacity of about 1.6 A·h/g. Samples **6** and **4** gave ∼38% and 19% increase in specific energy over a sample where carbon alone was used. Typically, cathodes that are machine-coated perform better than those coated by hand (method employed in this study). Increases in specific energy over 50% are expected with machine-coated cathodes using sample **6**. The enhancement in specific energy due to the electrocatalytic activity of γ-MnOOH obtained in this study is higher than that reported by Read[33] where a specific capacity of 0.7 A·h/g is obtained when λ-MnO_2 is incorpo-

(32) Calegaro, M. L.; Lima, F. H. B.; Ticianelli, E. A. *J. Power Souces* **2006**, *158*, 735−739.
(33) Read, J. *J. Electrochem. Soc.* **2002**, *149*, A1190.

rated in an air cathode using a current density of 0.1 mA/cm^2. The higher specific capacities exhibited by the synthesized manganite samples may be attributed to their much smaller sizes when compared to λ-MnO_2 used by Read.[34] The λ-MnO_2 used in Read's study was a micrometer-sized material (16 μm, 7 m^2/g) while the new manganite materials in this study were nanosized. The nanodimensions of the new manganite samples are evidently important and related to their higher specific capacities.

A unique lattice in the new manganite samples may also have formed as a consequence of the new preparation method reported in this study. Yang and Xu[35] reported that lattice distortions or defects significantly affect the electrocatalytic activity of manganese oxides. Similarly, while higher surface area among the synthesized γ-MnOOH here does not yield better electrocatalytic activity when compared to lower surface area γ-MnOOH, the degree of structural distortions might be the key to understanding the trend of activity observed in this report. We are currently studying this possibility by looking at structure refinements of the new manganite samples.

4. Conclusions

γ-MnOOH was successfully synthesized via a new route, which involved the reduction of $KMnO_4$ by sucrose and $MnSO_4$ in an acidic medium under refluxing conditions for 4 and 6 h. The reaction times are significantly lower than many recent synthetic pathways to γ-MnOOH which most of the time require hydrothermal conditions. Particle size seemed to be controlled by the mode of adding the three above-mentioned reagents. When $MnSO_4$ is added last to the reaction solution, a faster nucleation process is expected; hence, smaller particles could be obtained. Particle sizes of the new synthetic manganite materials (**4last** and **6last**) are smaller, hence, a higher surface area (62 and 63 m^2/g, respectively), when compared to one that is conventionally prepared (44 m^2/g). Manganite materials are important precursors to other important manganese oxides and lithium manganese oxides. TGA in air revealed that transformations of the new synthetic manganites to β-MnO_2, Mn_2O_3, and Mn_3O_4 are possible. Evaluation of the electrocatalytic activity in the reduction of O_2 of the synthesized manganite materials using cyclic voltammetry revealed higher peak currents (up to 6.4 mA) for larger particles, which provides further support for Bach's findings on the variation of electrochemical properties of manganese oxides with morphology, crystallinity, and bulk structure. When incorporated in the cathode of Yardney's medium-sized lithium-air battery as an electrocatalyst for the reduction of O_2 in air, sample **6** stood out as having a high promise for practical use, yielding a 38% specific energy increase (hand-coated method) over those where no manganite was incorporated.

Acknowledgment. We thank the Geosciences and Biosciences Division, Office of Basic Energy Sciences, Office of Science, U.S. Department of Energy, and Yardney Technical Products, Inc., for financial support. We thank Dr. Raymond Joesten and Dr. Abhay Vaze for useful discussions and Dr. Isabelle Lagadic for access to the diffuse reflectance infrared spectrometer.

CM062871Z

(34) Read, J.; Driedger, A.; Foster, D.; Wolfenstine, J.; Behl, W. *Electrochem. Solid State Lett.* **2001**, *4*, A162.
(35) Yang, J.; Xu, J. J. *Electrochem. Commun.* **2003**, *5*, 306−311.